

**Rationally structured triboelectric nanogenerator arrays for harvesting water current energy
and self-powered sensing**

Zichao Deng, Liang Xu, Huaifang Qin, Xianye Li, Jizhou Duan*, Baorong Hou, Zhong Lin
Wang**

Z. Deng, Prof. L. Xu, H. Qin, X. Li, Prof. Z. L. Wang

Beijing Institute of Nanoenergy and Nanosystems, Chinese Academy of Sciences, Beijing,
101400, P. R. China.

Z. Deng, Prof. J. Duan, Prof. B. Hou

Key Laboratory of Marine Environmental Corrosion and Bio-fouling, Institute of Oceanology,
Chinese Academy of Sciences, Qingdao, Shandong, 266071, P. R. China.

This article has been accepted for publication and undergone full peer review but has not been through the copyediting, typesetting, pagination and proofreading process, which may lead to differences between this version and the [Version of Record](#). Please cite this article as [doi: 10.1002/adma.202205064](https://doi.org/10.1002/adma.202205064).

This article is protected by copyright. All rights reserved.

Z. Deng, Prof. L. Xu, H. Qin, X. Li, Prof. J. Duan, Prof. B. Hou, Prof. Z. L. Wang

University of Chinese Academy of Sciences, Beijing, 100049, P. R. China.

Z. Deng, Prof. J. Duan, Prof. B. Hou

Open Studio for Marine Corrosion and Protection, Pilot National Laboratory for Marine

Science and Technology (Qingdao), Qingdao, Shandong, 266237, P. R. China.

Prof. Z. L. Wang

School of Materials Science and Engineering, Georgia Institute of Technology, Atlanta,

Georgia, 30332-0245, USA.

E-mail: xuliang@binn.cas.cn; duanjz@qdio.ac.cn; zlwang@gatech.edu

Abstract: Water current energy is an enormous and widely distributed clean energy in nature, with different scales from large ocean flow to small local turbulence. However, few effective technologies have been proposed to make use of different forms of water currents as a power source. Here, high-performance paired triboelectric nanogenerators (P-TENGs) capable of

integrating massively into a thin flexible layer as a structured triboelectric surface (STS) is demonstrated for harvesting water current energy. Novel gas packet exchange structure and rigid-flexible coupling deformation mechanism are introduced to ensure the device can work highly effectively even in deep water under high water pressure. The rationally designed TENG array in the STS enables highly efficient power take-off from the flow. Typically, the STS demonstrates high-frequency output up to 57 Hz, largely superior to current TENG devices, and the power density is improved by over 100 times for triboelectric devices harvesting current energy. The flexible STS is capable of attaching to various surfaces or applying independently for self-powered sensing and underwater power supply, showing great potential for water current energy utilization. Moreover, the work also initiates universal strategies to fabricate high-frequency devices under large environment pressure, which may profoundly enrich the design of TENGs.

Keywords: nanogenerator; water current energy; vortex-induced vibration; energy harvesting; underwater

1. Introduction

Different forms of water current widely distribute in rivers, lakes, and seas in our surrounding environment, which contains enormous energy to be exploited ^[1]. Usually, the uneven distribution of water temperature and salinity, or the effect of water surface wind, cause the flow of water and different velocities between deep and shallow water current ^[2]. Water current energy is a relatively stable type of clean and renewable energy source with great potential ^[3]. According to an estimation, the global available ocean current energy can reach 5 TW (1 TW = 10^{12} W), which may provide an important share in world clean energy supply for carbon neutrality ^[4]. Besides, the energy contained in small-scale water current of rivers and creeks can drive distributed environmental power sources for various applications far from the grid, without maintenance cost and pollution from chemical power sources ^[5]. This is especially crucial for deep-sea environment where other power sources, such as photovoltaic, are unavailable ^[6]. Currently, although large turbines based on electromagnetic generators

(EMGs) are constructed for harvesting large-scale water current energy in rivers, they have a relatively high requirement of water flow rate, which usually need a dam to raise the water level ^[7]. The attempts to harvest ocean current energy with turbines are found to be of high cost and low reliability ^[8]. Thus, there still lacks flexible technologies that can make use of different forms of water currents (even slow and in small scale) for power.

The emerging of triboelectric nanogenerators (TENGs) provides new opportunities to harness mechanical energies in the environment ^[9]. Based on the coupling of triboelectrification effect and electrostatic induction ^[10], the TENG can effectively convert mechanical energy into electricity, including wind energy, vibration energy, water droplet energy, water wave energy, and so on ^[11]. Compared with the EMG, the TENG exhibits merits of easy fabrication, cost-effectiveness, lightweight, diverse material and structure choices ^[5, 12]. Although a few studies have explored harvesting flow energy with TENGs, mostly in air, effective device designs remain to be sought due to challenges of power take-off (PTO) from unidirectional flow and tackling with water pressure that will squeeze structures together. Devices based on blades can effectively respond to unidirectional flow. However, they are usually large, complex, rigid, and hard to be integrated ^[13]. Flexible

flag-like TENGs based on vortex-induced vibration (VIV) have been reported to harvest both wind energy and underwater current energy, yet with relatively limited output due to the small internal mechanical strain or motion in the devices ^[14]. So great efforts are still needed to improve the electrical output and fill the gap for practical applications.

Here, high-performance paired triboelectric nanogenerators (P-TENGs) capable of integrating massively into a thin flexible layer as a structured triboelectric surface (STS) are demonstrated for harvesting water current energy based on vortex-induced vibration. Novel gas packet exchange structure of paired TENGs and rigid-flexible coupling deformation mechanism are introduced to ensure that the device can work highly effectively with contact-separation mode even in deep water under high water pressure. The rationally designed TENG array in the STS enables highly efficient power take-off from the flow compared with smooth surface when remaining a thin layer, converting unidirectional water current into high-frequency vibration and electrical output. Typically, with a thin TENG thickness of 4.5 mm, the STS demonstrates high-frequency output up to 57 Hz and high accumulated charge output of 1.59 $\mu\text{C/s}$ in water current of 2.2 m/s, largely superior to current TENG devices. The power density is improved by over 100 times for triboelectric

devices that harvest current energy. The flexible STS can be attached to various surfaces or applied independently underwater for self-powered sensing and underwater power supply, showing great potential for high-performance water current energy utilization and applications in deep-sea environments. Moreover, the work also initiates effective universal strategies for fabricating high-frequency TENGs and devices under large environment pressure, which may profoundly enrich the design of TENGs.

2. Results and Discussion

2.1. Fundamental structure and working principle of the STS

The basic concept of STS is demonstrated in **Figures 1a-c**. To harvest water current energy, the STS is designed as a thin flexible layer (Figure 1b) composed of small arrayed TENG cells with outreaching pillars (Figure 1c), which can interact with the water current and exchange energy. Multiple pieces of STSs can be arranged in parallel in the cross-section of the water current to maximize harvested energy and increase the power density by attaching to a multi-cavity framework underwater (Figure 1a). Water flows through the cavities and

transfers energy to the STS, which is converted into electricity for powering electronic devices. The design is rather flexible with high scalability using different amounts of cells in each STS, for different scales of water current energy harvesting and application. Considering the thin thickness of the STS, it can be arranged with high density, allowing high-power-density energy harvesting. Figure 1d demonstrates comparison of the STS with smooth surface in water current. When water flows over a smooth surface, they will have little interaction except frictional drag, with low energy exchange, thus little power take-off from the water current can be achieved. For the STS, water current will interact effectively with the surface structure and transfer energy to the TENG array in the surface for power generation. Compared with other devices for harvesting water current energy ^[7b, 13b], the STS is a rather thin layer with small volume and simple structure, flexible for attaching on different surfaces.

The detailed structure of a single cell of the STS is shown in Figure 1e, which is consisted of a TENG and auxiliary pillars as bluff bodies. The TENG is contact-separation mode with two layers. The upper layer adopts conductive silicone rubber (CSR) (carbon black (CB) mixed) as the electrode ($24 \times 24 \text{ mm}^2$), which is embedded into a silicone rubber (SR) substrate. The lower layer adopts Cu as the electrode and fluorinated ethylene propylene

(FEP) as the dielectric layer, which are attached to a polyethylene (PE) sheet and embedded into another silicone rubber substrate. Two PE pillars are attached to the upper layer via two trapezoidal PE sheets. More details of the fabrication process are described in the Experimental Section.

The upper and lower layers are bonded together and sealed for water-proofing as shown in Figure S1, Supporting Information. Two cells are paired together to form a functional module with a shared inner space, which is injected with air to enable a novel gas packet exchange mechanism for solving the challenge of large underwater pressure that will prevent separation of layers. For the first module in the inflow direction, extra pillars as initial bluff bodies are set for obtaining a better VIV effect in devices afterwards ^[15], which has been verified in experiments (Figure 1f). Trapezoidal PE sheets as a relatively rigid portion on the upper layer, together with the rest flexible portion of silicone rubber, allow the upper layer to deform into a controlled three-dimensional shape for proper layer separation. Detailed working mechanisms concerning the two novel designs will be introduced afterwards. Figure 1g shows the photographs of fabricated devices (two cells with the bluff body), which have excellent flexibility and can be attached to flat or curved objects.

Figure 1h presents the basic working mechanism of the TENG. Driven by the vibration of the pillars, the upper layer will deform to realize contact-separation motion, which is ensured even under high water pressure with aforementioned novel designs. The contact-separation motion of CSR and FEP films will cause surface charge separation due to triboelectrification, charging the surface of FEP film with negative static charges. Accompanying the contact-separation motion, free electrons will be induced to move between the two electrodes through an external circuit due to electrostatic induction (The arrow represents charge flow prior to the corresponding state). Then the mechanical energy can be converted to electricity.

2.2. Fundamental characterization of the TENG in air

To better understand the fundamental characteristics of the TENG, the device was tested first in air using a linear motor with regular agitation. As shown in **Figure 2a**, a triangular plate is driven by the linear motor to push the two pillars separate, which can restore contact by rubber bands. An angle θ is adopted to characterize the motion, which is defined as $\theta = (\theta_1 + \theta_2)/2$, where θ_1 and θ_2 are the angles between the two pillars and the substrate. The

open-circuit voltage (V_{OC}), short-circuit current (I_{SC}), and short-circuit transferred charges (Q_{SC}) for different motion amplitudes are shown in Figures 2b-d and Figure S2, Supporting Information. The device presents high sensitivity to external agitations of small amplitude. For typical motion angle range of $85^\circ - 100^\circ$, the peak-to-peak V_{OC} , I_{SC} , and Q_{SC} of a single cell can reach around 51 V, $0.76 \mu\text{A}$, and 18.5 nC respectively. Figure 2e shows the charging performance of a STS module to different capacitors. Typically, a $1 \mu\text{F}$ capacitor can be charged to 4.01 V in 15 s under an agitation frequency (f) of 5 Hz. Figure 2f shows the output of a single cell with different external loads. Maximum peak power of $46.8 \mu\text{W}$ is achieved at a matched load resistance of about $200 \text{ M}\Omega$.

2.3. Working mechanism and structure optimization of the device in water current

The STS harvests water current energy based on the VIV effect. As shown in **Figure 3a**, with proper conditions, vortices will form around the bluff body of the cell in the water current. Alternate shedding of vortices at the two sides of the pillar will impose an oscillating lift force and drag force on the pillar, inducing structural vibration, namely the VIV [16]. The Reynolds

number (Re) is a critical measure for the vortex shedding, which is defined as the following:

$$R_e = \frac{\rho U d}{\mu} \quad (1)$$

where ρ and U are the density and flow velocity of the fluid respectively; d is the characteristic length; μ is the dynamic viscosity.

Normally, the vortices will start to periodically shed when the Reynolds number is larger than around 40 [17]. The VIV of the pillars will further agitate the act of the TENGs, following the mechanism shown in Figure 1h. However, although the shown contact-separation of the TENG is normal in air without fully packaging the device, it is really difficult in water environment due to large pressure, which will prohibit separation of packaged layers. Due to such a reason, TENGs working underwater usually have small output because adequate separation is not achievable. To solve this problem, novel gas packet exchange structure of paired TENGs and rigid-flexible coupling deformation mechanism are designed to ensure that the device can work effectively with normal contact separation even in deep water under high water pressure.

As shown in Figure 3b, the two symmetric trapezoidal PE sheets are relatively rigid

portion on the upper layer, while the rest silicone rubber portion are flexible and elastic.

Following the externally agitated vibration of the pillars, the PE sheets also tend to oscillate.

Due to that the upper layer is bonded to the lower layer nearby, the long edge of the trapezoid is almost immovable. Meanwhile, the silicone rubber portion can deform well and act like a spring. Consequently, the two PE sheets can roll along the long edges of the trapezoids, which can be regarded as two virtual pivots, and the roll motion are synchronized due to the elastic silicone rubber between. Based on such coupling roles of the rigid and flexible portions, the upper layer can deform into a regular three-dimensional (3D) shape of a truncated pyramid as long as the inner pressure is balanced, allowing adequate layer separation for greatly enhanced output.

The contact-separation motion of the TENG is accompanied by a volume variation of the inner space, producing a pressure change in such packaged space, which will break the balance with outer water pressure and impose a high extra force to prevent contact-separation motion. To dynamically eliminate such negative effect, a novel gas packet exchange structure of paired TENGs is designed. As shown in Figure 3c, two TENGs are paired together with a shared inner space, and a small amount of air is encapsulated in as an

air packet that can exchange between the two TENGs. Such paired TENGs can work in a coordinated way, alternately entering the separation state via air packet exchange. Without such mechanism, the separation of the devices will be greatly suppressed. A circulating water tunnel system is adopted here for experimentally testing the device, where the device is mounted in a tunnel with controlled water current (Figure S3, Supporting Information). As shown in Figure 3d and Video S1, Supporting Information, the paired devices can work efficiently in water current with coordinated motion of the pillars and TENGs underneath. Figure 3e further compares the transferred charges of the TENGs with and without the gas packet. The one with the air packet has significantly higher output, implying adequate contact-separation of the TENG. Moreover, the gas packet can also be exchanged within multiple TENGs if they share the same inner space.

The geometrical design of the bluff body is crucial for its VIV response in water current, which is optimized, mainly concerning the diameter or edge length (D), length (L), and cross-sectional shape of the pillar (Figure S4, Supporting Information). The charge output of the rear cell with different diameters and lengths were demonstrated in Figures 3f, g. The results show that maximum outputs are achieved under a diameter of 4mm and a length of 25

mm, respectively. Then, the transferred charges of three cross-sectional shapes of round, square, and diamond were tested with a diameter or edge length of 4 mm and a length of 25 mm under different water flow velocities (Figures 3h-j). The round case shows relatively higher and stabler output which achieves about 24 nC under the flow velocity of 2.2 m/s, and the enlarged view is shown in Figure S5, Supporting Information. Thus, the device below will adopt cylindrical pillars with a diameter of 4 mm and a length of 25 mm unless otherwise specified.

2.4. Output performance of the device in water current

The performance of the cell with the optimized design is investigated in details in water current. **Figure 4a** shows the V_{OC} under different water flow velocities. It can be observed that the V_{OC} increases fast with the rise of flow velocity and tends to saturate at about 1.8 m/s, indicating that there may be a transition to adequate contact-separation motion. The V_{OC} can reach about 65 V at the flow velocity of 2.2 m/s, and the enlarged view is shown in Figure 4b. The I_{SC} presents similar trend and can reach about 7.2 μ A under the flow velocity of 2.2 m/s

(Figures. 4c, d). Considering the small size of the device, the high performance in water demonstrates the effectiveness of the device design.

Owing to the unique structure, the output of the device presents characteristics of high frequency, which can produce high rate of charge output. As shown in Figure 4e, the output frequency increases with the rise of the flow velocity, and reaches 57 Hz for the case of 2.2 m/s. Figure 4f presents the accumulated transferred charges per second (Q_{ac}) at different flow velocities, which are calculated according to the following equation:

$$Q_{ac} = \frac{\int_0^T |I| dt}{T} \quad (2)$$

where I is the output current, and T is the time span. As can be observed, when the flow velocity increases from 1.2 m/s to 2.2 m/s, the Q_{ac} enhances from 0.44 $\mu\text{C/s}$ to 1.59 $\mu\text{C/s}$. The performance achieved in this work is far beyond that reported in the literature. As shown in Figures 4g, h, the TENG in this work outputs much higher frequency and Q_{ac} with a small volume [11b, 18]. Considering that the output frequencies of most TENGs are decided by the external agitation frequency and can reach only a few Hertz, the STS provides an effective new strategy to fabricate high-frequency TENGs independent of external agitation frequency.

Moreover, the frequency response can be tuned based on the elasticity of the silicone rubber on the top layer, allowing responding to different ranges of water flow velocity.

Figure 4i demonstrates the charging performance of the paired TENGs, and a 33 μF capacitor can be charged to 0.78 V in 30 s. The output of the TENG under different external loads was also tested. As shown in Figure 4j, the peak value of the current decreases as the resistance rises. A maximum peak power of 193.4 μW at 20 $\text{M}\Omega$ and a maximum average power of 27.6 μW at 50 $\text{M}\Omega$ are achieved. Due to the increased operation frequency, the resistance for maximum power output is decreased in water experiments. The average power (P_{ave}) is calculated according to the following equation:

$$P_{\text{ave}} = \frac{\int_0^T I^2 R dt}{T} \quad (3)$$

where R is the resistance of the load. Meanwhile, the corresponding voltage output is demonstrated in Figure S6, Supporting Information. The power density of the device reaches 0.3357 W/m^2 in real water environment, which is more than 107.4 times of previous triboelectric devices and 5.6 times of piezoelectric devices for water current energy harvesting, respectively [14, 18b, 19] (Figure 4k). The output enhancement should be attributed to

the delicate structure design which enables highly effective power take-off and ensures adequate internal mechanical separation. Figure 4l shows the output of the device under long-term agitation of water current, which is stable with small enhancement, indicating outstanding durability.

2.5. Demonstration of the STS for applications

Owing to the design of small flexible cells, the STS is scalable for various applications concerning self-powered sensing and underwater power supply, based on water current energy of different scales ranging from large ocean current to small turbulence. **Figure 5a** shows a concept that the STS can be arranged in large arrays as an underwater power station, which can supply power for power consumers on the sea or underwater, such as oil platform, buoy, underwater vehicle and future underwater city. The diversion effect of the framework can ensure a suitable water flow direction. As a direct demonstration of excellent performance, 50 light emitting diodes (LEDs) can be lighted up by the small module under the agitation of water current (Figure 5b and Video S2, Supporting Information).

The TENG can be used directly as a self-powered water current sensor without external power supply, based on the good linearity between Q_{ac} and water flow velocity for devices with specific structure parameters, as shown in Figure 5c. The high output also enables the STS to power other electronics using water current as the power source. The corresponding circuit diagram is shown in Figure 5d. The front and rear cells charge the storage capacitor (C_s) after being rectified respectively, then the switch can be turned on to power the electronic device. Figures 5e, f show the self-powered temperature sensing system based on the module. A C_s of 220 μ F was charged to 2.35 V within about 136 s (There is also a small contribution from rectified environmental electromagnetic interference), then the switch was closed and a thermometer without battery was powered successfully. It is worth noticing that the voltage curve can remain stable afterwards, indicating that the harvested energy can supply the power consumption totally. Therefore, the thermometer can be powered continuously (Video S3, Supporting Information).

3. Conclusions

In this work, high-performance paired triboelectric nanogenerators capable of integrating massively into a thin flexible layer as a structured triboelectric surface are demonstrated for harvesting water current energy based on vortex-induced vibration. The device can work highly effectively with contact-separation mode even in deep water under high water pressure due to novel gas packet exchange structure and rigid-flexible coupling deformation mechanism. The rationally designed TENG array in the structured triboelectric surface enables highly efficient power take-off from the flow compared with smooth surface when remaining a thin layer, which converts unidirectional water current into high-frequency vibration and electrical output. With a thin TENG thickness of 4.5 mm, the device demonstrates high-frequency output up to 57 Hz and high accumulated charge output of 1.59 $\mu\text{C/s}$ in water current of 2.2 m/s, largely superior to current TENG devices. The power density is improved by over 100 times for triboelectric devices that harvest current energy. The flexible device can be attached on various surfaces or applied independently underwater for self-powered sensing and underwater power supply. Due to the ultra-small size of the device, it can be deployed in different scales as an array with large densities for practical applications, showing great potential for high-performance water current energy utilization

and applications in deep-sea environments. Moreover, the work also initiates effective universal strategies for fabricating high-frequency TENGs and devices under large environment pressure, which may profoundly enrich the design of TENGs and promote the application development towards related areas.

4. Experimental Section

4.1. Fabrication of the upper layer of the TENG

Firstly, the base and curing agent of silicone rubber (Ecoflex 00-30) were mixed in 1:1 weight ratio, which were then added conductive carbon black (Super P Li). The silicone rubber and conductive carbon black are in 9:1 weight ratio. After mixed uniformly, the mixture was smeared over a polyethylene terephthalate (PET) mold (1 mm in thickness), flattened with a piece of 2000-grit sandpaper and cured in an oven at 60 °C for 4 h. Then the conductive silicone rubber (CSR) was prepared. Afterwards, the CSR was removed from the mold and cut into a size of 24 × 24 mm² as CSR electrodes. Two CSR electrodes were put into another acrylic mold at specific positions. Uncured silicone rubber was poured into the mold and

cured at room temperature for at least 4 h. The silicone rubber layer with CSR embedded was then removed from the mold and smeared with powder (Johnson) partly for lowering stickiness.

4.2. Fabrication of the lower layer of the TENG

Firstly, a PE sheet ($24 \times 24 \times 0.5 \text{ mm}^3$) (fillet radius 4 mm), a copper tape (30 μm in thickness) and a FEP film (30 μm in thickness) were adhered together. Two such structures were put into the acrylic mold at specific positions. Uncured silicone rubber was poured into the mold and cured at room temperature for at least 4 h. The silicone rubber layer with the above structure embedded was then removed from the mold and smeared with powder (Johnson) partly for lowering stickiness. The bare FEP film was then corona charged with a voltage of 6 kV, and a duration of 15 min (ET2673A).

4.3. Fabrication of the STS

The upper and lower layers were bonded together and sealed for water-proofing using glue (5580), and more details on the position of bonding and packaging are shown in Figure S1, Supporting Information. Air was injected into the packaged space with a syringe and the

pinhole was sealed by glue (5580). Then, six PE pillars and trapezoidal PE sheets, which were shaped by a laser cutter (PLS 6.75, Universal Laser Systems), were attached to the upper layer using glue (5580) respectively.

4.4 Characterization of the device

The test in air was agitated by a linear motor (LinMot). A triangular plate was driven by the linear motor to push the two pillars separate, and rubber bands were used for restoring contact when the triangular plate drew back. A circulating water tunnel system was adopted for experimentally testing the device in water current. The experiment segment of the tunnel has a diameter of 10 cm, where the device was mounted. A pump (DSU-150) was used to generate water current in the tunnel, which was controlled by a frequency converter (ZK880-11KW). A flowmeter (BLD-DN100) was adopted for measuring the flow velocity. The open-circuit voltage, short-circuit current, and transferred charges were measured by an electrometer (Keithley 6514). A high-speed camera (Photron FASTCAM Mini AX) was applied to record the vibration state of the STS under the agitation of water current.

Supporting Information

Supporting Information is available from the Wiley Online Library or from the author.

Acknowledgements

Z. Deng and L. Xu contributed equally to this work. The research was supported by the National Key R & D Project from Minister of Science and Technology (2021YFA1201603, 2021YFA1201601), the Key Research Program of Frontier Sciences, CAS (ZDBS-LY-DQC025), the National Natural Science Foundation of China (No. 51605033, 51735001), and Youth Innovation Promotion Association, CAS (No. 2019170).

Conflicts of interest

The authors declare no competing interests.

Author Contributions

This article is protected by copyright. All rights reserved.

Z. D. and L. X. contributed equally. L. X. conceived the idea. L. X. designed the device and experiments. Z. D. fabricated the device. Z. D. did the experiments. Z. D., L. X., H. Q., and X. L. discussed the data and prepared the figures. L. X., Z. D., Z. L. W., and J. D. wrote and revised the manuscript. L. X., J. D., Z. L. W., and B. H. guided the project.

Received: ((will be filled in by the editorial staff))

Revised: ((will be filled in by the editorial staff))

Published online: ((will be filled in by the editorial staff))

References

- [1] a) J. Tollefson, *Nature* **2014**, *508*, 302-304; b) A. S. Bahaj, *Renew. Sust. Energy Rev.* **2011**, *15*, 3399-3416; c) N. Zdankus, P. Punys, T. Zdankus, *Renew. Sust. Energy Rev.* **2014**, *38*, 121-130.
- [2] H. Stommel, *Deep Sea Research (1953)* **1957**, *4*, 149-184.

[3] a) A. S. Bahaj, L. E. Myers, *Renew. Energy* **2003**, *28*, 2205-2211; b) Z. L. Wang, T. Jiang, L. Xu, *Nano Energy* **2017**, *39*, 9-23.

[4] a) Ocean current energy potential on the U.S. outer continental shelf, Minerals Management Service *Renewable Energy and Alternate Use Program*, U.S. Department of the Interior, **2006**; b) M. Salvia, D. Reckien, F. Pietrapertosa, P. Eckersley, N.-A. Spyridaki, A. Krook-Riekkola, M. Olazabal, S. De Gregorio Hurtado, S. G. Simoes, D. Geneletti, V. Viguié, P. A. Fokaides, B. I. Ioannou, A. Flamos, M. S. Csete, A. Buzasi, H. Orru, C. de Boer, A. Foley, K. Rižnar, M. Matosović, M. V. Balzan, M. Smigaj, V. Baštáková, E. Streberova, N. B. Šel, L. Coste, L. Tardieu, C. Altenburg, E. K. Lorencová, K. Orru, A. Wejs, E. Feliu, J. M. Church, S. Grafakos, S. Vasilie, I. Paspaldzhiev, O. Heidrich, *Renew. Sust. Energy Rev.* **2021**, *135*, 110253.

[5] L. Xu, L. Xu, J. Luo, Y. Yan, B. E. Jia, X. Yang, Y. Gao, Z. L. Wang, *Adv. Energy Mater.* **2020**, *10*, 2001669.

[6] Z. L. Wang, *Nature* **2017**, *542*, 159-160.

- [7] a) M. J. Khan, G. Bhuyan, M. T. Iqbal, J. E. Quaioco, *Appl. Energy* **2009**, *86*, 1823-1835;
b) L. I. Lago, F. L. Ponta, L. Chen, *Energy for Sust. Dev.* **2010**, *14*, 287-296.
- [8] M. Esteban, D. Leary, *Appl. Energy* **2012**, *90*, 128-136.
- [9] F. R. Fan, Z. Q. Tian, Z. L. Wang, *Nano Energy* **2012**, *1*, 328-334.
- [10] a) C. Wu, A. C. Wang, W. Ding, H. Guo, Z. L. Wang, *Adv. Energy Mater.* **2019**, *9*, 1802906; b) Z. L. Wang, J. Chen, L. Lin, *Energy Environ. Sci.* **2015**, *8*, 2250-2282; c) S. Niu, Z. L. Wang, *Nano Energy* **2015**, *14*, 161.
- [11] a) L. Xu, H. Wu, G. Yao, L. Chen, X. Yang, B. Chen, X. Huang, W. Zhong, X. Chen, Z. Yin, Z. L. Wang, *ACS Nano* **2018**, *12*, 10262-10271; b) W. Xu, H. Zheng, Y. Liu, X. Zhou, C. Zhang, Y. Song, X. Deng, M. Leung, Z. Yang, R. X. Xu, Z. L. Wang, X. C. Zeng, Z. Wang, *Nature* **2020**, *578*, 392-396; c) Y. Bai, L. Xu, C. He, L. Zhu, X. Yang, T. Jiang, J. Nie, W. Zhong, Z. L. Wang, *Nano Energy* **2019**, *66*, 104117; d) B. Chen, Y. Yang, Z. L. Wang, *Adv. Energy Mater.* **2018**, *8*, 1702649; e) H. Wang, L. Xu, Z. Wang, *Nanoenergy Adv.* **2021**, *1*, 32-57; f) J. Chen, Z. L. Wang, *Joule* **2017**, *1*, 480-521.

- [12] a) X. Li, J. Luo, K. Han, X. Shi, Z. Ren, Y. Xi, Y. Ying, J. Ping, Z. L. Wang, *Nat. Food* **2022**, *3*, 133-142; b) H. Qin, L. Xu, S. Lin, F. Zhan, K. Dong, K. Han, H. Wang, Y. Feng, Z. L. Wang, *Adv. Funct. Mater.* **2022**, 2111662; c) Z. L. Wang, *Mater. Today* **2017**, *20*, 74-82.
- [13] a) Z. Lin, B. Zhang, H. Zou, Z. Wu, H. Guo, Y. Zhang, J. Yang, Z. L. Wang, *Nano Energy* **2020**, *68*, 104378; b) Z. Wen, H. Guo, Y. Zi, M. H. Yeh, X. Wang, J. Deng, J. Wang, S. Li, C. Hu, L. Zhu, Z. L. Wang, *ACS Nano* **2016**, *10*, 6526-6534.
- [14] Y. Wang, X. Liu, T. Chen, H. Wang, C. Zhu, H. Yu, L. Song, X. Pan, J. Mi, C. Lee, M. Xu, *Nano Energy* **2021**, *90*, 106503.
- [15] G. R. S. Assi, J. R. Meneghini, J. A. P. Aranha, P. W. Bearman, E. Casaprima, *J. Fluids Struct.* **2006**, *22*, 819-827.
- [16] a) T. Sarpkaya, *J. Fluids Struct.* **2004**, *19*, 389-447; b) C. H. K. Williamson, R. Govardhan, *Annu. Rev. Fluid Mech.* **2004**, *36*, 413-455.
- [17] J. H. Lienhart. Synopsis of lift, drag, and vortex frequency data for rigid circular cylinders. Washington State University, College of Engineering, *Research Division Bulletin* **1966**, *300*.

- [18] a) J. Wang, S. Li, F. Yi, Y. Zi, J. Lin, X. Wang, Y. Xu, Z. L. Wang, *Nat. Commun.* **2016**, *7*, 12744; b) Y. Wang, X. Liu, Y. Wang, H. Wang, H. Wang, S. L. Zhang, T. Zhao, M. Xu, Z. L. Wang, *ACS Nano* **2021**, *15*, 15700-15709; c) Z. Ren, Z. Wang, Z. Liu, L. Wang, H. Guo, L. Li, S. Li, X. Chen, W. Tang, Z. L. Wang, *Adv. Energy Mater.* **2020**, *10*, 2001770; d) X. Yang, L. Xu, P. Lin, W. Zhong, Y. Bai, J. Luo, J. Chen, Z. L. Wang, *Nano Energy* **2019**, *60*, 404-412.
- [19] a) U. Latif, E. Uddin, M. Y. Younis, J. Aslam, Z. Ali, M. Sajid, A. Abdelkefi, *Energy* **2021**, *215*, 119195; b) R. Song, X. Shan, F. Lv, T. Xie, *Ceram. Int.* **2015**, *41*, S768-S773; c) X. Shan, R. Song, B. Liu, T. Xie, *Ceram. Int.* **2015**, *41*, S763-S767.

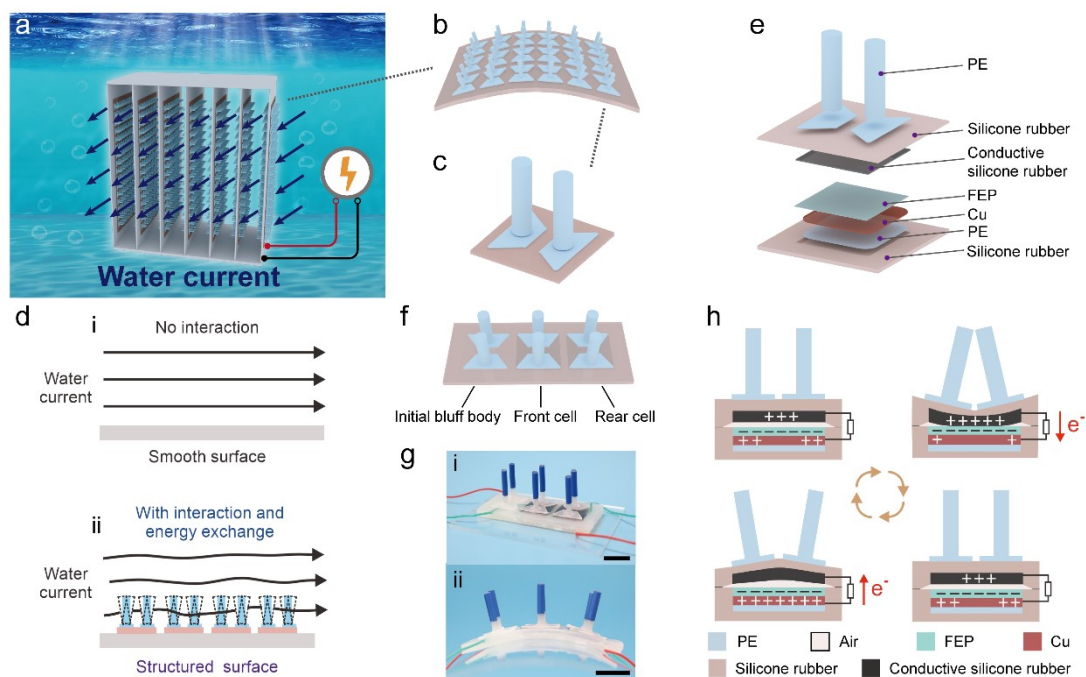


Figure 1. Fundamental structure and working principle. a) Schematic illustration of multiple pieces of the structured triboelectric surface (STS) for harvesting water current energy. b, c) Schematic illustrations of a piece of STS (b) and a single cell of the STS (c). d) Comparison of water flowing through smooth surface and structured triboelectric surface. e) Explosive view of a single cell. f) Schematic illustration of the STS module with the initial bluff body. g) Photographs of the as-fabricated STS. Scale bar: 20 mm. h) Working principle of the TENG.

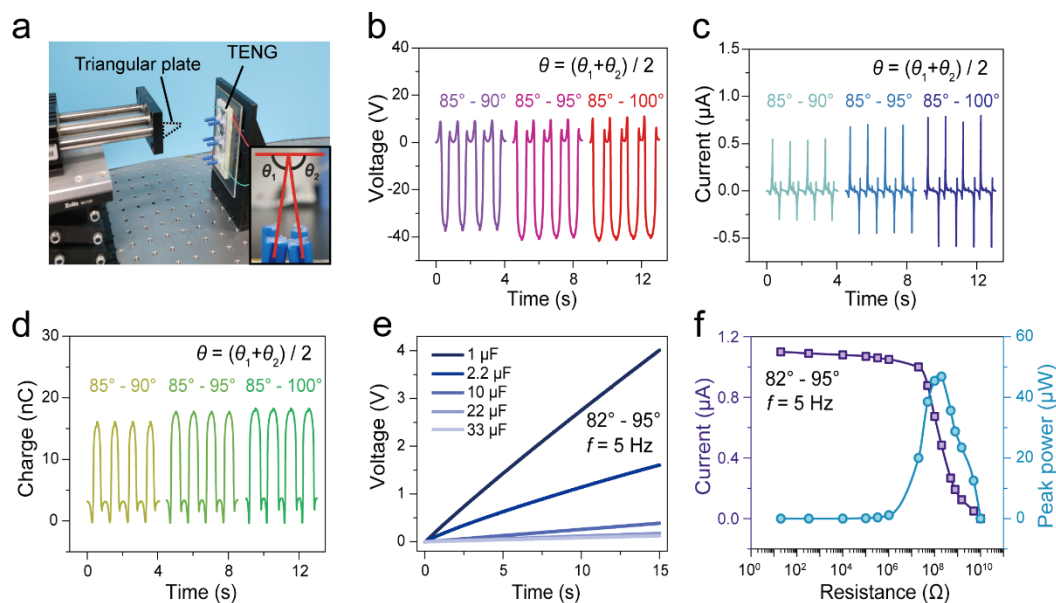


Figure 2. Fundamental characterization of the TENG in air. a) Photograph of the experiment setup. Inset: Angles for characterizing the motion amplitude. b-d) Open-circuit voltage (b), short-circuit current (c), and transferred charges (d) of a single cell with different motion amplitudes. e) Charging performance of a STS module to different capacitors. f) Peak current and peak power of a single cell with different external loads.

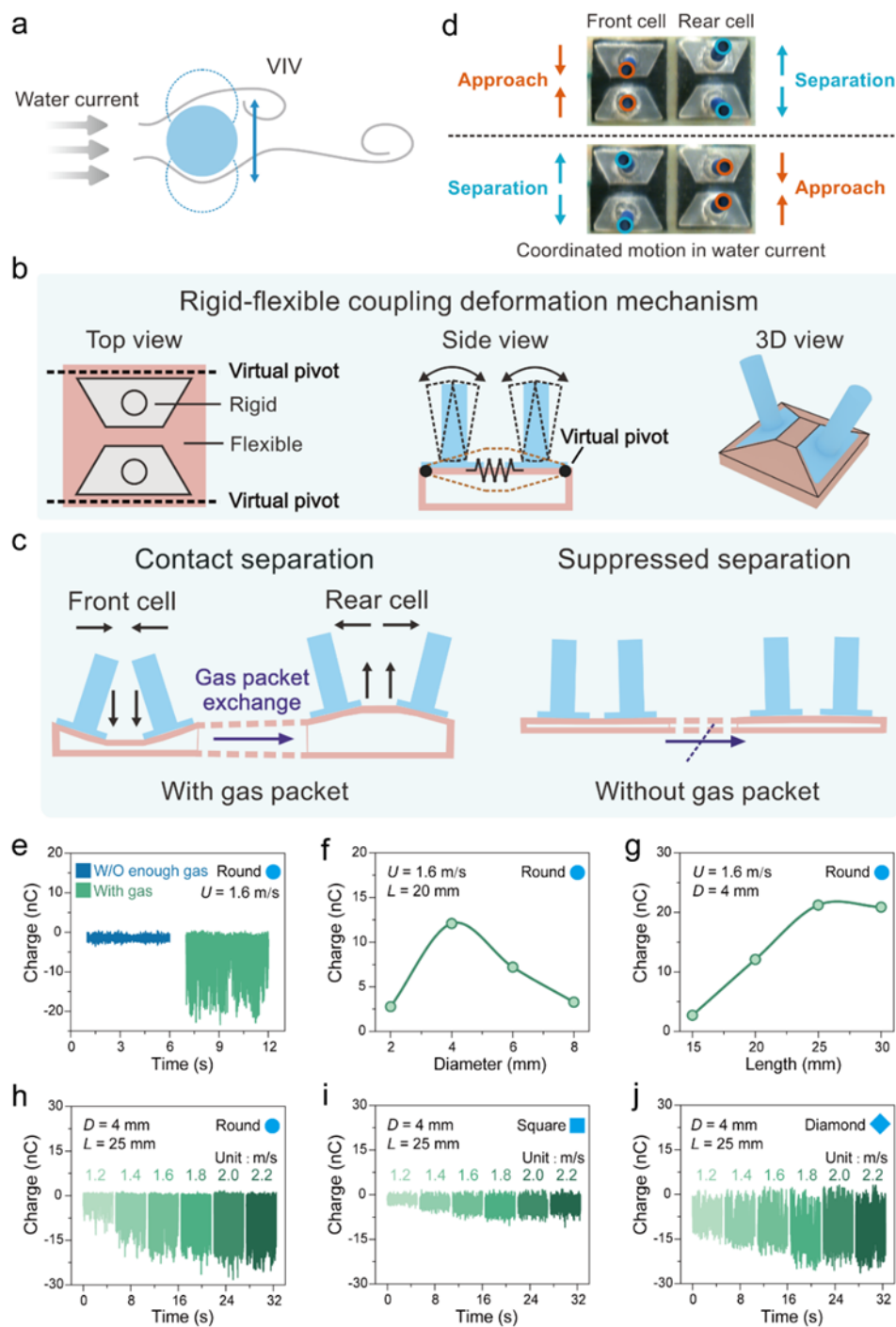


Figure 3. Working mechanism and structure optimization of the device in water current. a)

This article is protected by copyright. All rights reserved.

Schematic diagram of vortex-induced vibration (VIV) in water current. b) Schematic diagram of rigid-flexible coupling deformation mechanism. c) Effect of gas packet exchange between paired TENGs. d) Photographs of coordinated motion states of paired TENGs. e) Transferred charges of the rear cell with and without (W/O) the gas packet. f, g) Transferred charges of the rear cell with different pillar diameters (f) and lengths (g). h-j) Transferred charges of the rear cell with round (h), square (i) and diamond pillars (j).

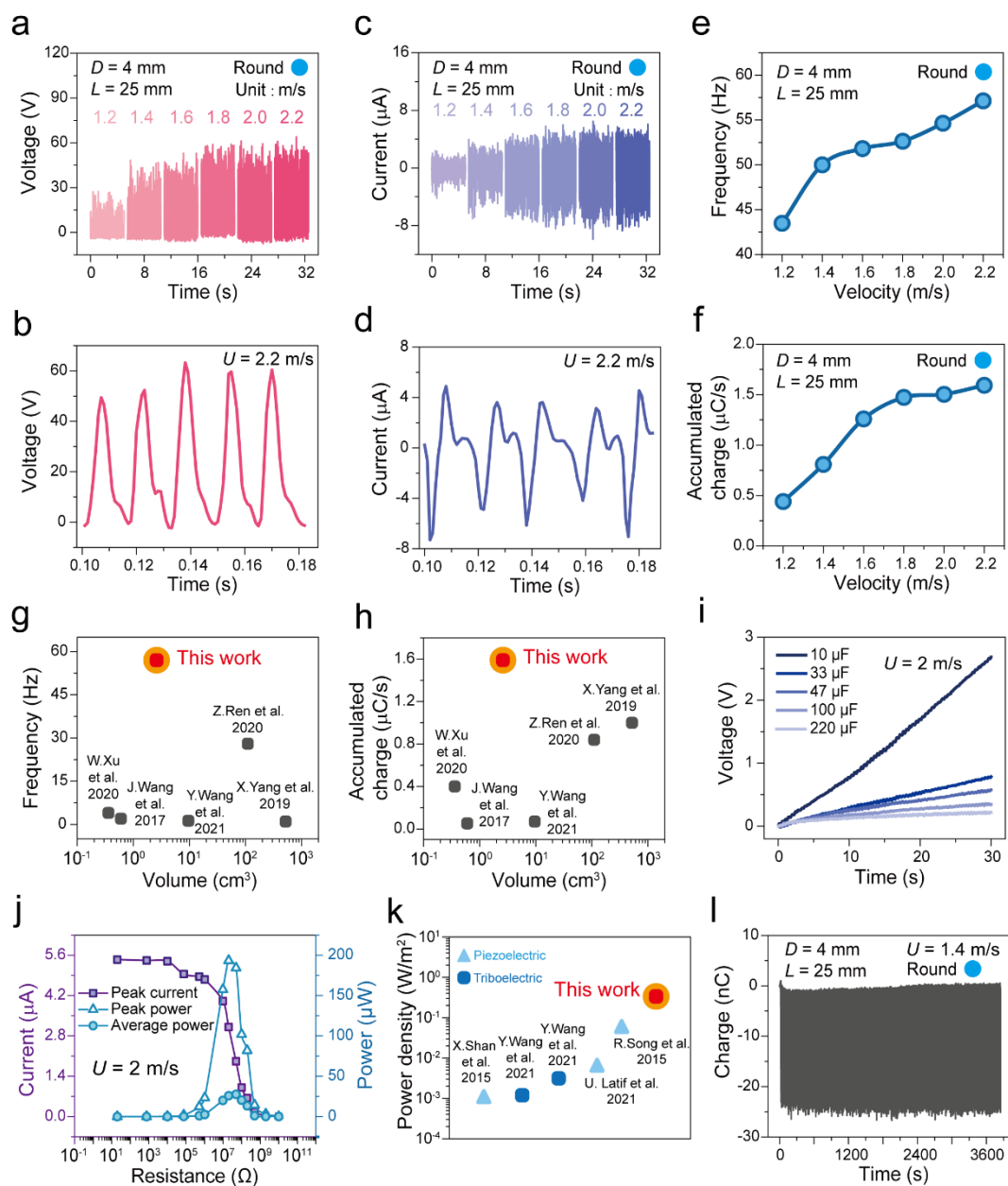


Figure 4. Output performance of the device in water current. a, b) Open-circuit voltage of the rear cell under different water flow velocities (a) and the enlarged view at 2.2 m/s (b). c, d) Short-circuit current of the rear cell under different water flow velocities (c) and the enlarged

view at 2.2 m/s (d). e) Vibration frequency of the rear cell under different flow velocities. f)

Accumulated transferred charges per second of the rear cell under different flow velocities. g,

h) Comparison of output frequency (g) and accumulated transferred charges per second (h)

with previous reported results [11b, 18]. i) Charging performance of the paired TENGs to

different capacitors. j) Output current and power of the rear cell with different external loads. k)

Comparison of power density with previous reported results for harvesting water current

energy [14, 18b, 19]. l) Durability of the cell in water current.

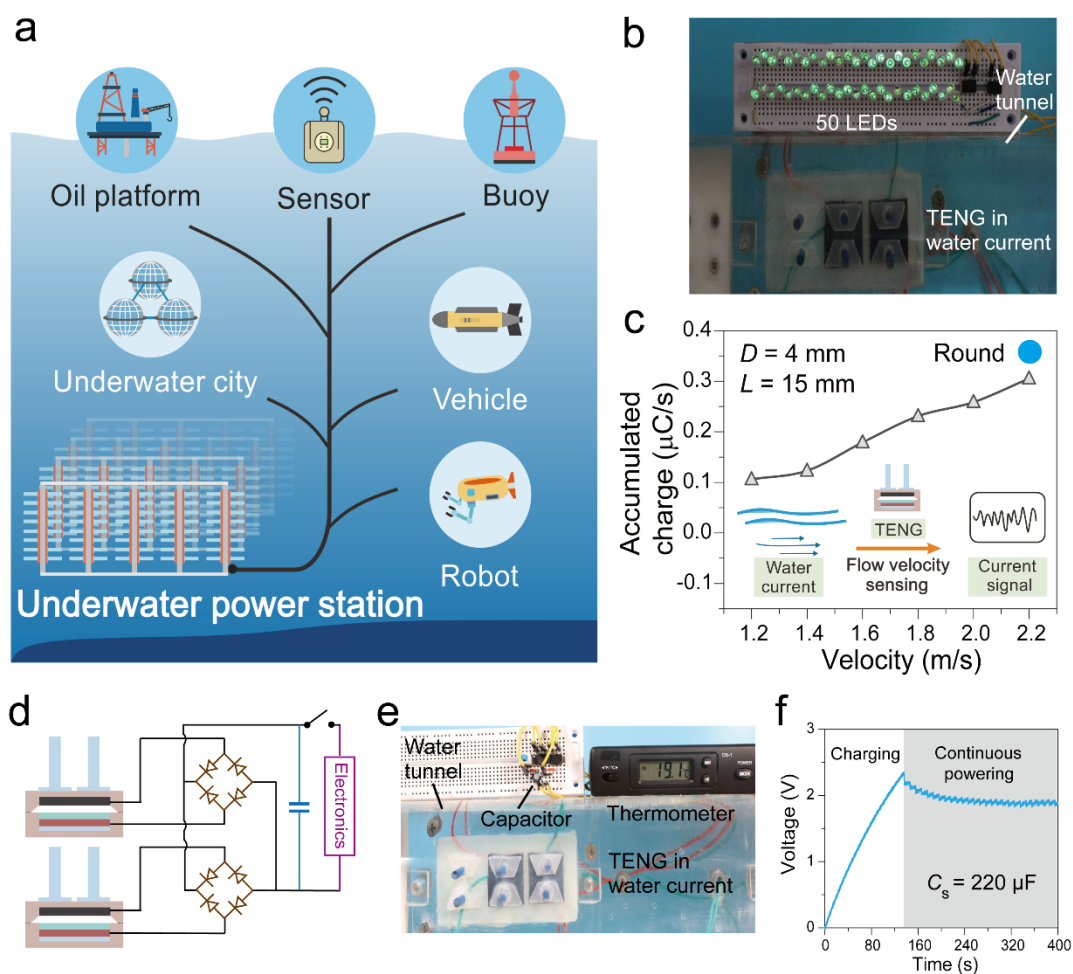


Figure 5. Demonstration of the STS for applications. a) Schematic perspective of the underwater power station. b) Photograph of 50 LEDs lighted up by the STS module. c) Relationship of accumulated transferred charges per second and water flow velocity for sensing. Inset: Schematic diagram of self-powered flow velocity sensing. d) Circuit diagram of the STS module for powering electronic devices. e, f) Photograph of the STS module continuously powering a thermometer (e) and the corresponding voltage curve of the storage

capacitor (f).

Paired nanogenerators capable of integrating massively into a thin flexible layer as a

structured triboelectric surface are demonstrated for harvesting water current energy.

Through novel gas packet exchange structure and rigid-flexible coupling deformation

mechanism, the device can work effectively even in deep water with greatly enhanced

performance, providing universal strategies to fabricate high-frequency TENGs under large

pressure.

Zichao Deng, Liang Xu*, Huaifang Qin, Xianye Li, Jizhou Duan*, Baorong Hou, Zhong Lin

Wang*

Rationally structured triboelectric nanogenerator arrays for harvesting water current energy

and self-powered sensing

